Gait Measurement with Acceleration Sensors

Peter van Alem[1], Peter Bakker, Larisa Gomaz[2], Anastasiia Hraivoronska[3], Suzanne Indenkleef[1], Mia Jukić[4], Rico Lammers[1], Scott Marquis[5], Michael Muskulus[6], Mark Peletier[3], Vivi Rottschäfer[4], Mara Smeele[4], Steve Taylor[7]

Abstract

Within the framework of the ShoQR project, Tim Gerbrands is interested in the analysis of human motion with acceleration sensors. In particular, the challenging problem is to infer the knee load during a patient walking. In this report, we investigate ways to extract meaningful information about human gait using the acceleration sensors. Our first approach is applying frequency domain analysis techniques to the sensor measurements. Secondly, we propose a couple of mathematical models of the leg that captures the quality of the knee. Furthermore, we examine the capabilities of the sensors by performing new experiments.

[1]Fontys University of Applied Sciences, The Netherlands
[2]Delft University of Technology, The Netherlands
[3]Eindhoven University of Technology, The Netherlands
[4]Leiden University, The Netherlands
[5]University of Oxford, England
[6]Norwegian University of Science and Technology, Norway
[7]University of Auckland, New Zealand

KEYWORDS: ShoQR, IMU sensors, gait analysis

3.1 Introduction

ShoQR is a health care research project led by Tim Gerbrands at the Fontys Paramedical University of Applied Science. The project objective is quantifying the shock-absorbing properties of the legs.

3.1.1 Tim Gerbrands and the ShoQR project

Tim Gerbrands is a specialist in human motion and especially gait analysis. The modern technology supporting motion analysis includes various advanced tools such as 3D motion capture, videotaping with high-speed cameras, force plate measurements, and electromyographic measures of muscle activity. Naturally, the equipment is expensive and the measurements can only be done in a laboratory. An alternative considered by Gerbrands is to use cheap and compact motion sensors that can be placed on a human body. The sensors should be convenient enough to allow physiotherapists or people with motion disorders to own personal sensors and to use them outside a laboratory. On the other hand, this approach raises the question of how to use the sensors in a way that is useful for gait analysis and how to extract meaningful information from data from this type of sensors.

To study what can be gained from the sensor data, we need to understand what aspects of human gait are of interest for researchers and therapists. While walking, people follow a repetitive pattern that is known as the gait cycle. Every step we make begins with a heel strike. At that moment, we experience a ground reaction force; consequently, a shock wave is initiated at the foot and propagates through the body. The shock absorption in the body correlates with the risk of injuries and can be of particular importance for people with motion disorder. One of the main research lines in the ShoQR project led by Gerbrands concerns the shock absorption and measuring it with the sensors.

A particular application of ShoQR measurement devices that could be realised is to help physiotherapists to treat patients with knee osteoarthritis. A manifestation of osteoarthritis is damaged or degen-

erated knee cartilage. Therefore, a standard recommendation for the patients is to reduce the load of joints and especially avoid overload. For this purpose, a clinically feasible measurement instrument that allows obtaining information on joint load can be extremely useful. Such measurements can support training of patients by giving information for adapting the walking style to reduce the load on the knees. Moreover, it could give warnings if the load is close to the danger threshold.

Previous experiments with the ShoQR measurement devices have shown that it may be possible to obtain statistically different outcomes for people with healthy and damaged cartilage. Nonetheless, the relation between the measurement and the quality of cartilage is not well understood. The challenge proposed by Gerbrands is to build a mathematical model to estimate joint loading and predict joint tissue damage. His suggestion was to describe a leg as a series of springs or spring-dampers with adjustable mechanical properties.

The sensors give a lot of freedom in their usage, and at the same time, the data obtained from measurements requires critical interpretation. We look at the description of sensors in the next section.

3.1.2 Description of the sensors

Gerbrands uses *Trigno Avanti* sensors made by the company Delsys[8] (see Figure 3.1). These sensors consist of an Inertial Measurement Unit (IMU) and a component that measures muscle activation. In this report we only use the data from the IMU.

Figure 3.1: The Avanti sensors used by Gerbrands.

[8] https://www.delsys.com/products/

An IMU consists of three parts: an accelerometer, a gyroscope, and a magnetometer. Each produces three scalar outputs: the accelerometer outputs acceleration in three directions, the gyroscope rotational velocity around three axes, and the magnetometer for the vectorial magnetic field.

The sensors used by Gerbrands can read at the maximum frequency of 470 Hz, and provide all three types of output. The sensors are read wirelessly, allowing them to be attached to the body without restricting movement. The orientations of the sensors are chosen in the way to measure the longitudinal and transversal components of acceleration as shown in Figure 3.2.

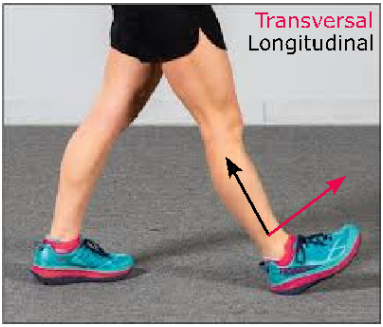

Figure 3.2: Depiction of the longitudinal and transversal axis.

3.1.3 How we interpreted the challenges

After several discussions we decided that the best interpretation of the question posed by Gerbrands is the following:

> *Can we extract clinically relevant information from IMU sensor measurements?*

We identified the following subquestions:

1. *What clinically relevant information can we deduce from frequency-dependent behaviour?*

Our starting point for this question is the data from Gerbrand's previous experiments with the sensors (Section 3.2.1). We focus on the measurements taken while a person was walking and standing on a vibration plate. The primary step for extracting relevant information is to reduce uncertainty and noise in the raw data. We overview useful prepossessing steps, namely mapping to the global coordinate system and removing noise in Section 3.2.2.

What can be clinically valuable information is a relation between the signal from the ankle and the lower back that allows for distinguishing people with healthy and damaged knees. We study frequency domain analysis methods that can give such a relation for the normal gait data in Section 3.2.3. We also investigate if the vibration plate data can provide information on the health of joints in Section 3.2.4.

We used the opportunity to perform our experiments with sensors and record the data during some participants of our group walking (Section 3.4.1). That gave us the freedom to experiment with the position of the sensors.

2. *Can we infer material properties of the knee cartilage?*

   We attempt to quantify the quality of the cartilage in two models of the leg (Sections 3.3.2 and 3.3.3). In the first model, we assume cartilage to be a viscoelastic medium. Then we expect the viscosity parameter to measure the material property. In the second approach, we model a knee as a spring with a damper; thus, we relate the spring stiffness and the dissipation coefficient with the material property. In both cases, the idea is to solve the inverse problem: estimate these model parameters for given measurements.

   Taking into account the complexity of the human body, we propose to examine the capabilities of IMU sensors by doing well-controlled experiments. For instance, we discuss an experiment with wood and foam representing bones and cartilage in Section 3.4.2.

3. *Can we determine forces in the knee during walking?*

This question is of particular practical interest because, as mentioned in Section 3.1.1, reliable information about the load of knees would help to treat the patients. However, determining forces in the knee is challenging and gives direction for further investigation. We make a small step in that direction because the leg model presented in Section 3.3.2 allows determining the stress in the knee.

3.2 Data exploration

3.2.1 Data received from previous experiments

We received data from Gerbrands' previous experiments. In these experiments, three IMU sensors were attached to the ankles and the lower back of patients. Each sensor is attached to bare skin to minimize the influence of clothing on the measurements.

Gerbrands' reasoning for positioning the sensors on these positions is that he expects to find a relation between the forces that act on the ankles, the lower back, and the knee. No sensor is put on the knee itself because it restricts movement. There is soft tissue directly above the knee that influences the measurements, so the hip is the closest to the knee position where soft tissue does not influence the measurements too severely. If the force that acts on the ankles and the hip can be measured, we might be able to determine the amount of absorption of the shock by the knee. The idea is that there might be a relation between the difference in force between the ankles and the hip and the condition of the patient's knee-cartilage.

We analysed data of different tests on one person. Each dataset describes one of these tests. In each dataset, time series with different frequencies are included. The datasets include data from roughly 30 seconds measured at 148 Hz.

The different datasets describe the different tests that were executed:

- Normal gait
- Running gait

- Asymmetric gait
- Jump
- Right legged jump
- Vibration plate with straight legs
- Vibration plate with bend knees
- Vibration plate with pointed toes.

The data was obtained from a person without damaged cartilage; we did not receive data from patients with damaged cartilage. Furthermore, information such as gender, height, and weight are not included in the data.

We focused on the dataset describing the normal gait. In Figure 3.3 the accelerations in the longitudinal and transversal axis of one walking cycle from one ankle for different timestamps are given. Moreover, the phases of the walking cycle (from touchdown of the right foot to the next touchdown of the right foot) are given below the data.

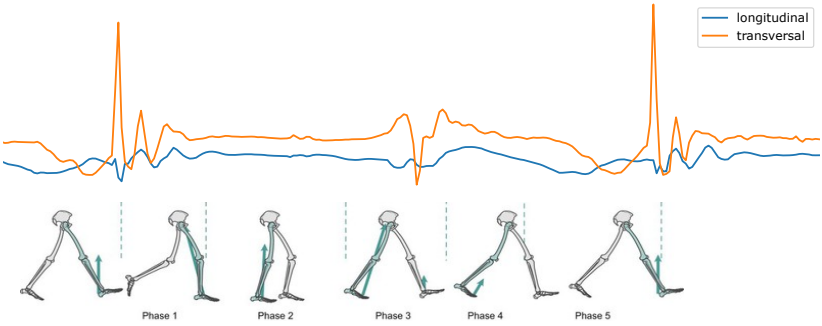

Figure 3.3: Acceleration in the longitudinal (blue) and transversal (orange) axis.

It can be seen that a large acceleration is measured when the patient puts the heel on the ground. The leg goes from a backward motion to a stop when the heel touches the ground, resulting in a forward force. This explains the large acceleration peaks.

3.2.2 Sensor fusion and removal of artifacts

The main data that are used are acceleration signals measured along three axes. It is important to realize that the coordinate system is fixed relative to the sensor and not a global one. This has the effect that the rotation of the sensor unit (e.g. during motion) will result in changes in the axes along which signals are being measured.

There are simple ways to deal with this, at least in principle. First, the local character of the measurement coordinate system can even be advantageous, e.g., when accelerations acting in the longitudinal direction along the leg are of interest. Provided that the sensors are oriented sensibly and accurately when attached for the experiments, a single acceleration signal could be used. Second, if the signal of interest is dominating the measurements, e.g., if the signal to noise ratio is suitably high, one can use the resultant length of the acceleration vector, i.e., the acceleration norm.

What complicates this, however, is the fact that the sensors also measure the local gravitational acceleration - unfortunately this is roughly of the same order of magnitude as the signals of interest. Rotation of the sensor, either due to motion of the body, or due to motion relative to it, changes the direction of the local gravity vector. This will be apparent even in the otherwise invariant acceleration norm, since depending on direction the gravity vector can increase or decrease the magnitude of the total acceleration. It is, therefore, desirable to remove the gravitational acceleration from the measurements prior to using the data.

This is one reason that IMU sensors contain not only accelerometers but additional sensors. A tri-axial magnetometer senses the orientation of the local magnetic field. Given that this field varies slowly over typical distances in our application scenarios, this is in principle sufficient to estimate and correct measurements for the gravitational acceleration. However, the magnetometer signals are influenced by magnetic materials, and indoor measurements are not very reliable by itself. The sensors are therefore complemented by gyroscopes that measure angular velocities.

Measurements with such an IMU are subject to noise (e.g. thermal), and obtaining reliable orientation and/or position estimates is

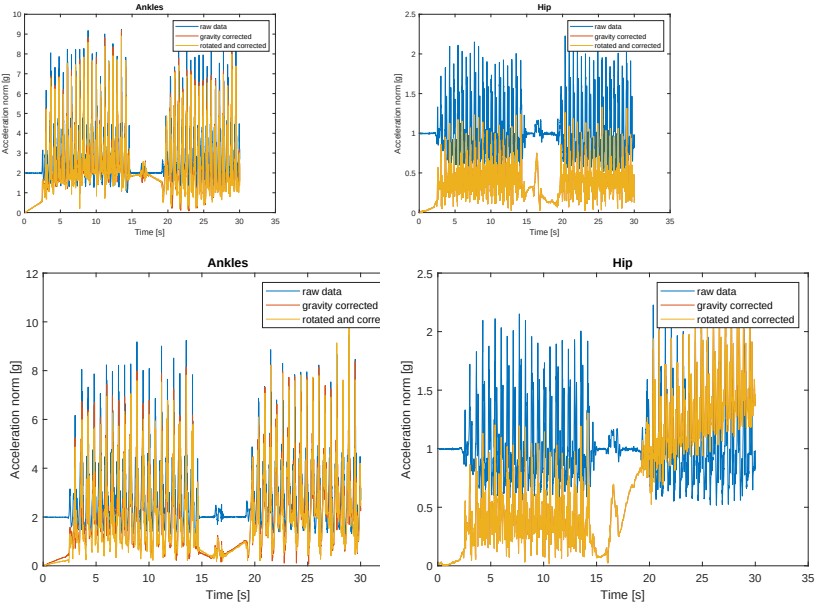

Figure 3.4: Correction of sensor data. Example shows acceleration norms of combined ankle and hip time series. Top row: Reconstruction of accelerometer data using gyroscope data (MATLAB function *imufilter*). Bottom row: Reconstruction using both gyroscope and magnetometer data (MATLAB function *ahrsfilter*).

a challenging problem of data fusion, especially if no direct position measurements (e.g. from a GPS unit) are additionally available. The usual approach is based on assuming a noise and sensor model and using a time-series filter. Variants of the Kalman filter have proved to be relatively well understood and straightforward to implement for this problem Madgwick, Harrison, and Vaidyanathan (2011) and Kok, Hol, and Schön (2018). A number of algorithms are readily available in the MATLAB Sensor Fusion and Tracking Toolbox Roetenberg et al. (2005) and Valenti, Dryanovski, and Xiao (2015).

Figure 3.4 shows an example of data correction by sensor fusion during walking. The gravity vector contributes $1g$ to the hip signal and $2g$ for the ankles signal, which is the vector sum of the signals from both ankles. Its influence is clearly visible in the raw data at stand-still (blue curves, initial part and middle segment). Subtracting the estimate of the gravity vector leads to the other curves (red and orange superimposed; the acceleration norms of the corrected signals in the two different coordinate systems are identical). The quality of the reconstruction is far from perfect and depends on the reconstruction algorithm. For example, including the magnetometer data (bottom row) leads to a better reconstruction of the ankles signal, but the hip signal starts to drift in the second half of the walk. Only using the gyroscope data (top row) avoids this problematic issue, but leads to an overall worse identification of the gravity vector.

Due to these shortcomings and because of lack of time, we have performed no sensor fusion and measurement correction in our analyses. Note that when vibrations are of interest (e.g. in the frequency domain analyses performed), a change in the mean level of the signals can be neglected, as long as it is acting slowly enough.

3.2.3 Frequency domain analysis

It is reasonable to investigate a relation among different signals from IMU sensors in the frequency domain rather than in the time domain because of the periodic nature of the walking data. For instance, one can use the power spectral density. Power spectral density is a frequency decomposition of the variance of a signal Bendat and Piersol (2011). Gerbrands made the observation that the ratio between the power spectral density of the ankle and lower back can give information about the state of cartilage. In Henriksen et al. (2008) they use the following "transfer function" relating the power spectral densities of the lower back PSD_{back} and of the ankle PSD_{ankle}

$$TF = 10 \log_{10} \left(\frac{PSD_{back}}{PSD_{ankle}} \right). \tag{3.1}$$

Gerbrands observed that the following transfer function differs significantly between people with healthy knees and with damaged knee car-

tilage.

There are different ways to preprocess signals from IMU sensors. One way is to calculate the Euclidean norm of the accelerations on the ankle and lower back before the data is transformed into the frequency domain. This way it does not matter how the sensor is orientated. We use the acceleration data in the transversal direction (Figure 3.2) because we think the transversal direction gives the most information. A disadvantage of this method is that a small difference in the orientation of the sensor will influence the results.

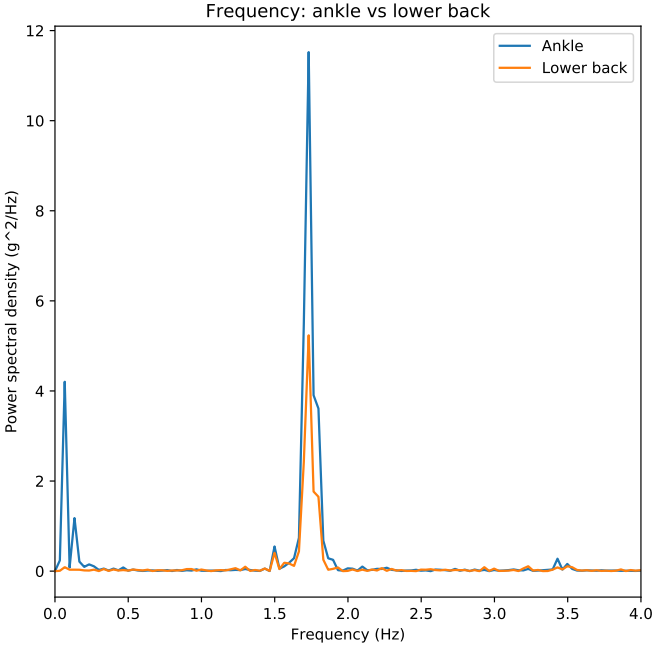

Figure 3.5: Power spectral density of lower back signal and ankles.

First, we will apply the same method as Gerbrands to see if we can reproduce the results. We obtain the power spectral density (Figure 3.5). To compare them Gerbrands calculated the ratio between the heights of the peaks. We suggest calculating the area under the graph rather than the height of the peak in order to reduce the calculation error. In particular, in our approach, we do not need to extract the frequency corresponding to the peak.

To seek further confirmation that there is a relation between the signal from the ankles and the signal from the lower back, we take a look at the coherence between the two signals. Coherence is a number between 0 and 1 which can be used to examine the relation between two signals. The higher the number, the stronger the correlation between the two signals.

At different frequencies, the coherence between the signals is defined as

$$C_{xy} = \frac{|P_{xy}|^2}{P_{xx} \cdot P_{yy}}. \tag{3.2}$$

Here, C_{xy} is the coherence between two signals x and y, P_{xx} and P_{yy} are the power spectral density estimates of the two signals, and P_{xy} is the cross spectral density estimate of the two signals Bendat and Piersol (2011). Welch's method is used to compute the power spectral densities Welch (1967).

In Figure 3.6 we show the coherence and the power spectral density. Notice that the power spectral density is outside the visible range. The frequency of the peaks is more important than the height of the peaks. The coherence shown in Figure 3.6 is the coherence between the Euclidean norm of the accelerations from the lower back and the Euclidean norm of the accelerations of the ankles. One can observe that at the dominant frequency the coherence is high. The harmonic frequencies, depicted by the smaller power spectral density peaks in Figure 3.6, also have relatively high coherence.

According to Henriksen et al. (2008) it is of interest to consider the power spectral density for the frequencies higher than the walking frequency because the effect of the cartilage can be seen for 6-20 Hz. In Figure 3.7 one can notice that the coherence is high for the frequency approximately 7 Hz.

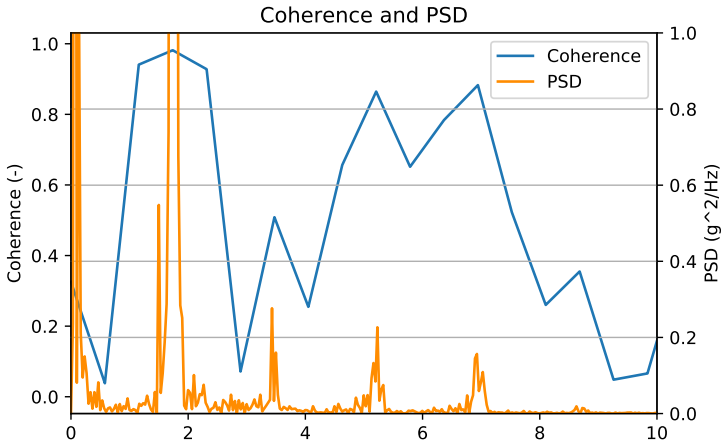

Figure 3.6: Coherence and Power Spectral Density of the ankles signal

We recall that the idea of the frequency domain analysis is to find a relation between the signal from the ankle and the lower back such that allows us to infer the quality of cartilage. We suggest using the coherence to examine the relation. However, to make any conclusion about this approach one has to apply it to a large amount of data that allows one to make statistically significant conclusions.

3.2.4 Is it possible to get useful information from vibration plate data?

Vibration plates are used for exercise programs. They are designed to vibrate the body while the subject maintains certain positions or movements. These machines are relatively inexpensive, so the study group was asked to investigate their potential usefulness as a tool to extract information about the health of joints in the human body. Specifically, we were provided accelerometer data, as described in Section 3.2.1, for a person standing on a vibration plate. The goal is to see if this data can

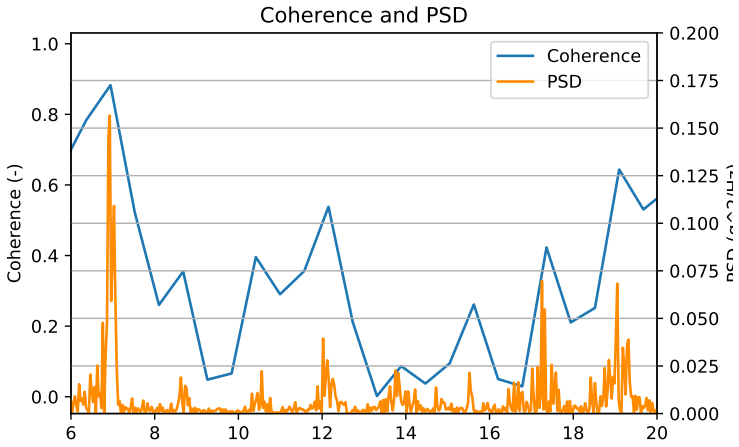

Figure 3.7: Coherence and Power Spectral Density of the ankles signal at 6 to 20 Hertz

provide information about the joints by using it to estimate parameters for a model of the body, such as those discussed later in Section 3.3.

The vibration plate has a platform on which the subject stands. The platform moves vertically in an oscillatory fashion. It is important to note that the platform moves in such a manner that each leg is moving in a direction opposite to that of the other leg. Thus, if the left leg is moving upwards, then the right leg is moving downwards, and vice versa. Data for two different postures were provided; standing with straight legs and standing with bent legs. Accelerometers were attached as close as possible to bony parts of the body in an attempt to measure the movements of the bones and avoid spurious movements of the soft tissue.

Figures 3.8 and 3.9 show Fourier transforms of the acceleration measurements of the vibration plate, the ankle, and the lower back, for straight and bent legs respectively. The frequency of vibrations is approximately 7 Hz. We observe that the amplitudes of the knee accelera-

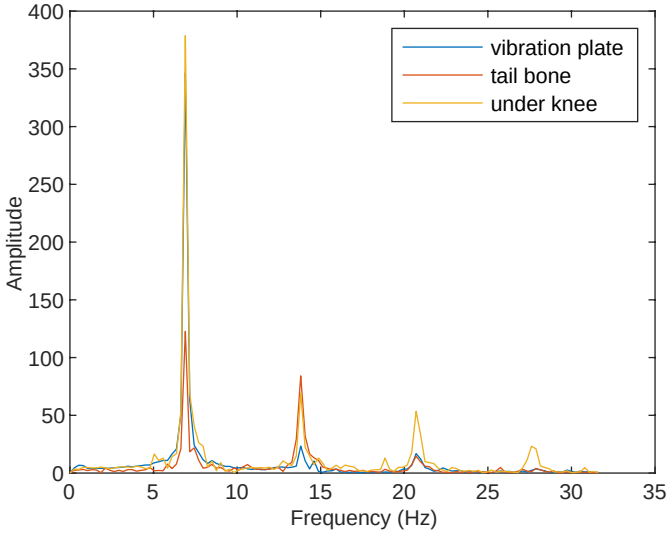

Figure 3.8: Fourier transform of vertical accelerations for a person on a vibration plate with straight legs.

tions at this frequency are larger than those of the vibration plate itself, indicating that the system is close to its resonant frequency. However, the amplitudes of the tailbone oscillations at this frequency are smaller than those of the vibration plate. This is explained by the fact that the sensor at the lower back is positioned at the tailbone and this is midway between the two legs. The legs are moving in opposite directions, so the acceleration of any part of the body midway between the two legs is expected to be smaller. We also observe that the system has significant responses at 2, 3 and 4 times the forcing frequency. The presence of these higher modes of vibration indicates a nonlinear response to the forcing.

The resonance effects that we observe in the data are not surprising when one considers that the vibrating plate is designed for exercise by vibrating the muscular tissue of the body as much as possible.

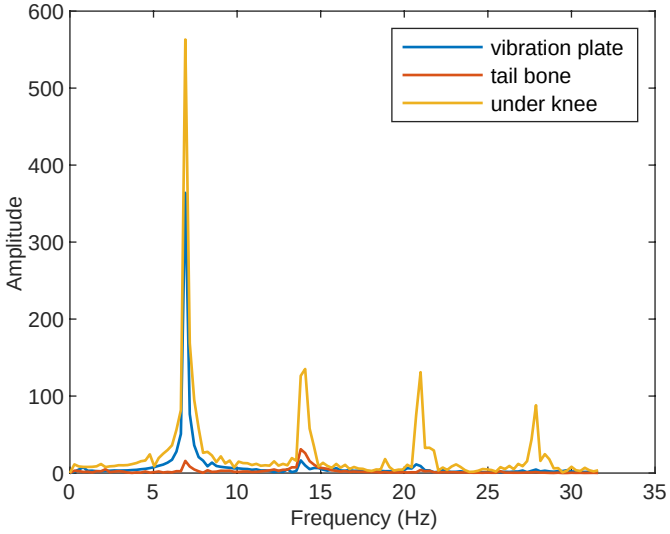

Figure 3.9: Fourier transform of vertical accelerations for a person on a vibration plate with bent legs.

Large scale movement of this soft tissue is accompanied by large scale movement of the skin. Thus this resonance behaviour dominates the measurements and we get no useful information about the joints.

It may well be worth considering different frequencies. Harazin and Grzesik (1998) investigate the response of standing humans in various postures when the subjects are standing on plates vibrating at a range of frequencies. These authors also observe a resonance close to the 7 Hz frequency. For frequencies less than this, they remark that "individual body parts are linked and behave as one resultant mass in the region of the main resonance frequency". It follows that frequencies less than 7 Hz would also not be useful to us.

We must therefore conclude that using a vibrating plate to generate data useful for the analysis of joints would require frequencies higher than the approximately 7 Hz of a standard vibrating plate. For

frequencies around 7 Hz, the soft tissue movement dominates the measurements. Harazin and Grzesik (1998) find that soft tissue movement is damped at higher frequencies, so it might be possible to extract useful information at a sufficiently high frequency.

3.3 Models

In the section, we attempt to understand how to develop a model of the leg that captures the material properties of the knee cartilage. We begin by investigating the physics background of wave propagation from ankle to hip during walking. The important question is what role the cartilage plays in wave propagation. Furthermore, we present two physics-based mathematical models of the legs.

In the first model (1D straight-leg model), we neglect the inherent complexity of walking and instead opt to consider a straight leg. In this straight-leg model, we capture the critical viscoelastic response of each component of the leg. By combining the straight-leg model with experimental data obtained by applying an impact force to a patient's straightened leg, we propose a simple method for determining critical knee cartilage parameters, which we hypothesise to be correlated with the health of a patient's knee.

The second model (two-segment leg model) neglects the detailed viscoelastic response of the various elements of the leg and instead considers the bending of a knee. In this model, the upper and lower leg are treated as rigid bodies whilst the rotational effects of the knee ligaments are captured by a spring and dashpot element. We presume the damping coefficient of the dashpot to be correlated with quality of cartilage. The focus of this model is to recover the change in angle between the upper leg and lower leg during walking.

3.3.1 Physics background

From the physical point of view a walking cycle includes processes with different time scales. Acceleration data from IMU sensors show a spiky, relatively high-frequent shock at the time of heel strike when walking. This spiky signal is superimposed on the recordings of smooth,

relatively low-frequent movements of walking. Besides high-frequent shocks and low-frequent steps, the role of muscles and tendons should be considered, because they play an important role in shock absorption. Experiments conducted in Konow and Roberts (2015) show that the time-rate of build-up and release of forces by muscles and tendons is slower than that of the fluctuations of the ground force, although they constrain the movement of the bones to some extent.

The high-frequent oscillations in the IMU data are seen as a shock, propagating from ankle to hip following principles of (visco-)elastic wave propagation. To understand the physical meaning of wave propagation in the human leg we will introduce the basics of wave propagation theory for a thin and sufficiently long elastic rod. Amirkulova (2011) shows that there exist waves with displacement merely in the longitudinal direction, namely *compressional guided waves*, and *flexural waves* with displacements almost entirely in a uniform transverse direction. Recall the directions shown in Figure 3.2 and see the illustration of waves in Figure 3.10.

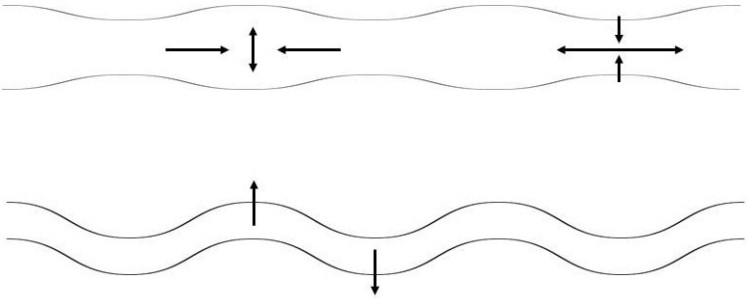

Figure 3.10: Particle displacements for a longitudinal, compressional guided wave (above) and a flexural wave (below).

A longitudinal, compressional guided wave occurs in case of uniaxial stress, and is described by the following wave equation,

$$E\frac{\partial^2 u_L}{\partial x^2} - \rho\frac{\partial^2 u_L}{\partial t^2} = F,$$

where u_l is the dominant displacement along the longitudinal x-axis (subscript L stands for longitudinal), E is Young's modulus, ρ is density, t is time, and F is an external force. Via Poisson's ratio (typical value of 0.3), there is also a sub-dominant component of displacement in the transverse radial direction. The propagation velocity of longitudinal, compressional guided waves is expressed by $v_L = \sqrt{E/\rho}$. Now we can estimate the propagation velocity in bones by using typical elasticity parameters as found in Van Buskirk, Cowin, and Ward (1981): $E \approx 9.7$ GPa and $\rho = 1000$ kg/m3, and hence $v_L = 3000$ m/s. Note that one may find a rather wide range of values for E reported in the literature. For instance, Ghosh et al. (2017) report a value of $E \approx 17$ GPa for tibia (frontal bone in the lower leg). However, the order of magnitude is rather consistent.

Flexural waves have a displacement component u_T (and acceleration $\partial^2 u_T/\partial t^2$) in a uniform transverse direction, perpendicular to the longitudinal axis of the rod. The other components of particle displacement almost vanish. Thus, a flexural wave follows a shear movement in the plane spanned by the relevant transverse direction and the longitudinal axis of the rod.

Such a flexural wave satisfies the Euler-Bernoulli beam equation (e.g. see Hörchens (2010) for an elaborate derivation),

$$\frac{\partial^4 u_T}{\partial x^4} + \frac{\rho A}{EI}\frac{\partial^2 u_T}{\partial t^2} = F,$$

or refinements thereof (Rayleigh beam theory or Timoshenko beam theory), describing infinitesimal bending of the rod. Here, u_T is the particle displacement in a transverse direction, x is the coordinate along the longitudinal axis of the rod, t is time, and the coefficient in front of $\frac{\partial^2 u_T}{\partial t^2}$ includes Young's modulus E, density ρ, the cross-sectional area of the rod A, and $I = \int z^2 dA$ is the area moment of inertia (z is the coordinate in the relevant transverse direction, relative to a 'neutral surface' in the centre). Solving this equation in the frequency domain leads to a phase velocity of $v_F = \sqrt{\omega}\left(\frac{EI}{\rho A}\right)^{1/4}$. For a circular cross-section of the rod, $I = \frac{\pi}{4}R^4$ where R is the radius of the rod, and $A = \pi R^2$. To estimate the wave velocity in the tibia bone we take a radius of 2 cm, with E and ρ as before, and substituting $\omega = 2\pi f$, we get $v_F =$

$5.6\sqrt{\omega} = 14\sqrt{f}$ m/s. At a frequency of 25 Hz (as a dominant shock frequency in ShoQR IMU acceleration data), this implies a flexural wave velocity of 70 m/s. This value is considerably lower than flexural velocities reported in the literature for human tibial bones, measured at higher frequencies.

The flexural waves have the property that the amplitude strongly decays with propagation distance. This dispersive property is illustrated in several experiments. With two accelerometers at 10 cm distance Girrbach et al. (2001) measured velocities in a range of 220-250 m/s for signals excited by a hammer. Aygün et al. (2015) measure dominant frequencies of 558.4 Hz, 285.2 Hz, 294.4 Hz and 288.5 Hz for an impact hammer under the knee and with an accelerometer placed at 5, 10, 15 and 20 cm distance from the hammer, respectively. A dominant frequency of 127.1 Hz is measured at the ankle. At a frequency of 300 Hz, the analysis above leads to a velocity of 242 m/s, which is reasonably consistent with these values in the literature. In their work, Bruin et al. (2005) measure velocities of 426 - 464 m/s for an impact hammer and a short distance between two accelerometers (10 a 15 cm). The majority of measurements by Vogl et al. (2016) is also in this range, with a central frequency of 3 kHz.

These numerical values of velocities and frequencies of flexural waves show that the typical wavelengths in the context of the ShoQR experiments are much larger than the length of a human leg. Hence, accurate modelling of the dynamics of wave propagation in a leg is extremely difficult. Due to the long wavelengths in comparison to the length of the leg, the (uncertain) boundary conditions will play a dominant role. It may be more appropriate adopting a quasi-static point of view, where stress and strain are in equilibrium, and the dynamics is completely controlled by source excitation.

The geometry of bones and joints is significant for physical modelling. We consider the role of the interfaces between cartilage and bones in the knee. Very clear illustrations (including a video) of the knee can be found in Meyler (2018). During normal walking, the cartilage is compressed and sheared.

The displacements at the interface between cartilage and tibia plateau (after integrating accelerations over time twice) are decomposed into a longitudinal component u_L (associated with compressional guided wave

propagation, with an additional radial component via Poisson's ratio) and a transversal component u_F, associated to flexural wave propagation. The longitudinal compressional guided wave goes with a single stress component $\sigma_{L,m}$ which is normal to the interface. This component is continuous across the interface, and relates to normal strain by Young's modulus, $\sigma_{L,m} = E\epsilon_{L,m}$. Typical values of compressive modulus in human cartilage (typically 2 - 10 MPa, see Setton, Elliott, and Mow (1999)) are orders of magnitude smaller than for bones. Thus, for propagation of compressive waves cartilage acts as a cushion (with relatively large strain) between the upper and lower leg. Since the upper leg is not moving freely, boundary conditions at the hip largely reduce the amount of energy transferred from the lower leg to the upper leg.

Similar arguments hold for the displacements and stresses associated to a flexural wave. Assuming that the transversal component u_F is the only non-zero component of the particle displacement vector, there is only one non-zero shear strain component, $\epsilon_F = \frac{1}{2}u_{F,n}$, which is related to the associated shear stress by $\sigma_F = G\epsilon_F$, where G is the dynamic shear modulus (assuming isotropy). For healthy cartilage, Setton, Elliott, and Mow (1999) and Wong et al. (2008) report values of G in order of magnitude of 0.26 - 0.5 MPa, which is orders of magnitude lower than the shear modulus of tibia (e.g., 6.5 GPa is reported by Ghosh et al. (2017)). So, cartilage also acts as a cushion between the upper and lower leg for transmitting shear stress and associated particle displacement. Interesting shear experiments on cartilage tissue are reported by Wong et al. (2008), showing that cartilage elastic properties vary with depth from the top surface at which shear traction is applied in their experiments. A thin surface layer is weaker, leading to decay of shear strain as a function of depth. Moreover, fluids play an important role as lubricant.

Osteoarthritis tends to considerably reduce the compressive and shear moduli of cartilage. Setton, Elliott, and Mow (1999) reports reductions up to 65% for E and up to 45% for G, and Wong et al. (2008) reports a reduction by a factor of 3 for G in the surface layer in an initial phase of osteoarthritis. This might be a plausible, partial explanation of the findings in the ShoQR project of the substantially stronger amplitude attenuation of measured hip IMU accelerations for patients suffering from osteoarthritis, relative to healthy persons (im-

pact reduction of 87% versus 57%).

Furthermore, it should be noted that cartilage is known to be a visco-elastic tissue, see Fulcher, Hukins, and Shepherd (2009). We will build 1D straight-leg model (Section 3.3.2) assuming that the wave propagates in the knee as in linearly visco-elastic medium. This means that the stress $\sigma(t)$ is not just linearly related to strain $\varepsilon(t) = \frac{\partial u}{\partial x}$ by elasticity parameters (e.g., $\sigma(t) = E\varepsilon(t)$ with Young's modulus), but it also depends linearly on strain rate $\frac{d\varepsilon}{dt}$. It is convenient to use a complex-valued extension of the elasticity parameters $E = E' + iE''$, where E' is known as the storage modulus, and E'' is known as the loss modulus. Then the stress is

$$\sigma(t) = E'\varepsilon(t) + \frac{E''}{\omega}\frac{d\varepsilon}{dt}.$$

Note that if the strain is harmonic, thus can be expressed in the form $\varepsilon(t) = \varepsilon_0 \sin(\omega t)$ with some amplitude ε_0 and frequency ω, then the associated stress is expressed by

$$\sigma(t) = \varepsilon_0 E' \sin(\omega t) + \varepsilon_0 E'' \cos(\omega t).$$

It is common practice expressing the amount of viscosity by the loss angle $\delta = \tan^{-1}(E''/E')$. Fulcher, Hukins, and Shepherd (2009) measure values of $\delta \approx 5°$. Little seems to be known about relationships between cartilage viscosity and osteoarthritis, except from the fact that lubricant fluids in the knee tend to be less viscous for patients suffering from osteoarthritis (see Conrad (2001)).

3.3.2 1D Straight-Leg Model

In this section, we introduce our 1D model of a straight leg. We divide the leg into three sub-domains: the lower leg (LL), the knee (K), and the upper leg (UL) and also couple our leg model to a simple model of the upper body (UB), see Figure 3.11. We denote the length of each domain by L_i with i = LL, K, UL, UB. Note that the model is one dimensional model with x is in the horizontal direction in Figure 3.11. The time between detection of a signal at the lower back and the ankle is very short, therefore we assume that bone is the main medium of propagation in both the lower and upper legs. However, in the knee,

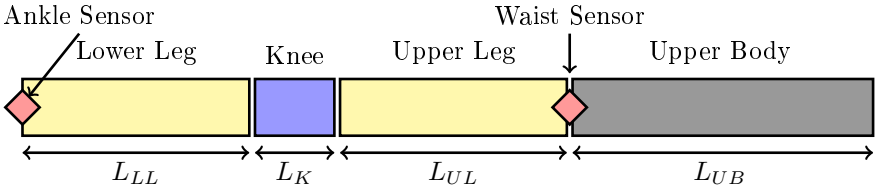

Figure 3.11: Schematic of 1D leg and upper body model.

there is no bone and therefore we expect that cartilage is the main medium of propagation. In our model, we consider longitudinal, compressional guided wave propagation through each sub-domain and treat each material (bone and cartilage) as viscoelastic, assuming a constitutive law of Kelvin-Voigt form. A Kelvin-Voigt consists of a spring and a dashpot (viscous damper) in parallel. The upper body is also treated as a viscoelastic material with a Kelvin-Voigt constitutive law but we consider this too as a collection of multiple bones, cartilage, etc in the upper body. Therefore, for a displacement u_i, we take the governing equations in each sub-domain ($i = \text{LL, K, UL, UB}$) to be

$$\rho_i A_i \frac{\partial^2 u_i}{\partial t^2} = \frac{\partial}{\partial x}\left(A_i \sigma_i\right), \tag{3.3a}$$

$$\sigma_i = E_i \frac{\partial u_i}{\partial x} + \eta_i \frac{\partial}{\partial t}\left(\frac{\partial u_i}{\partial x}\right), \tag{3.3b}$$

where ρ_i, A_i, E_i, and η_i are the density, area, Young's modulus, and viscosity of the material of propagation in sub-domain i. Here, σ_i is the Cauchy stress. We have neglected any effects of the foot in this model but this could be incorporated using another viscoelastic model similar to those in the other sub-domains. Therefore, we apply a force $F(t)$ at the ankle. We model this by the boundary condition on the left boundary of the lower leg

$$A_{LL}\sigma_{LL}(0,t) = F(t). \tag{3.4a}$$

We also enforce continuity of displacement, and a force balance at the

boundaries between each sub-domain. Therefore, we take

$$u_{LL}(L_{LL},t) = u_K(L_{LL},t), \quad A_{LL}\sigma_{LL}(L_{LL},t) = A_K\sigma_K(L_{LL},t), \tag{3.4b}$$

$$u_K(L_{LL}+L_K,t) = u_{UL}(L_{LL}+L_K,t), \tag{3.4c}$$
$$A_K\sigma_K(L_{LL}+L_K,t) = A_{UL}\sigma_{UL}(L_{LL}+L_K,t), \tag{3.4d}$$

$$u_{UL}(L_{LL}+L_K+L_{UL},t) = u_{UB}(L_{LL}+L_K+L_{UL},t), \tag{3.4e}$$
$$A_{UL}\sigma_K(L_{LL}+L_K+L_{UL},t) = A_{UB}\sigma_{UL}(L_{LL}+L_K+L_{UL},t). \tag{3.4f}$$

For simplicity, we also assume that the upper body will damp out all disturbances before the top of the upper body. Therefore, we impose zero displacement at the top of the upper body

$$u_{UB}(L_{LL}+L_{LK}+L_{UL}+L_{UB},t) = 0. \tag{3.4g}$$

Finally, we assume that every component of the leg is initially undisplaced and stationary. Therefore, for $i = \text{LL, K, UL, UB}$, we have

$$u_i(x,0) = 0, \quad \frac{\partial u_i}{\partial t}(x,0) = 0. \tag{3.4h}$$

Model Parameters

Our ultimate goal is to fit a single parameter, namely, the damping coefficient of the knee, η_K, to the accelerometer data at the lower back when we employ the accelerometer data at the ankle as in input. However, the 1D leg model contains 20 unknown parameters and so we must provide typical values for the remaining 19 parameters. In this section, we explain the reasoning behind the parameter values that we have chosen but it should be noted that these values are just rough estimates and should be refined. In particular, we use the parameters for bone in the upper body but it is probably more realistic to take lumped/averaged cartilage and bone values. The parameter values that we use in our simulations are given in Table 3.1.

As a first approximation, we simply take a rough order of magnitude estimate of the lengths of the lower leg, knee, upper leg, and upper body. These can easily be refined by measuring a particular patient or average person.

In the lower leg, upper leg, and upper body we simply take the densities to be given by the typical density of bone as reported in John and Cameron (1999). In the knee, we employ the density of cartilage reported in It'is (2010 (accessed June 2, 2020)). The values should be refined depending upon a patient's age etc.

In the lower leg, upper leg, and upper body we find the cross-sectional area of the conducting material to be given by a bone with a 3 cm radius via the expression $A = \pi r^2$. We recommend that these numbers are refined by neglecting the bone marrow in the inner bone and also by obtaining more accurate values that capture the difference in the upper and lower leg bones as well as a more accurate averaged value in the upper body. These can be obtained by finding average values of bone thicknesses in each sub-domain. For the cartilage, we take the cross-sectional area to be given by a disc with a radius 1 cm, which is less than the cross-sectional area of a bone to represent the fact that not every part of the cross-sectional area of the bone is in contact with the cartilage.

For Young's modulus in the lower leg, upper leg, and upper body, we use a typical value for Young's modulus of cortical bone Rho, Ashman, and Turner (1993). For the Young's Modulus of the cartilage we take a value provided by Gerbrands. The viscosity values that we have chosen in each region are rough estimates based on bone and cartilage values we obtained from the literature.

Normal stresses

An important aspect of the model is that after solving the proposed equations numerically, one can determine the normal stress at the joints. We draw attention to this because potentially, this allows inferring the force in the knee caused by applying a force F at the ankle. Recall that the stress is defined by the equation (3.3b):

$$\sigma_i = E_i \frac{\partial u_i}{\partial x} + \eta_i \frac{\partial}{\partial t}\left(\frac{\partial u_i}{\partial x}\right).$$

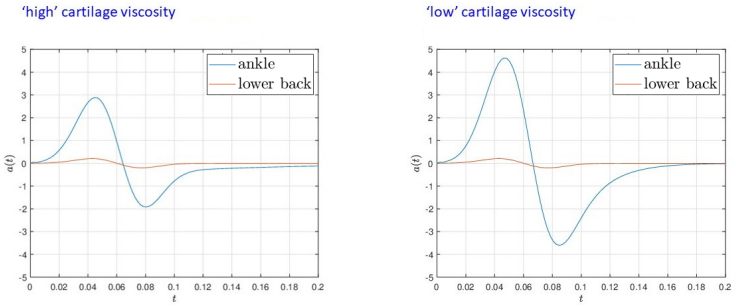

Figure 3.12: Comparison of high viscosity cartilage ($\eta_K = 2 \times 10^6$ $\mathrm{kg\,m^{-1}\,s^{-1}}$) and low viscosity cartilage ($\eta_K = 1 \times 10^6$ $\mathrm{kg\,m^{-1}\,s^{-1}}$).

The model is capable of examining the amount of normal stresses at the cross-section of each joint between domains as a result of peak impacts. This allows investigating whether the joint load represented by those stresses is under the danger threshold.

Impulse Response

In Figure 3.12, we present impulse response results from the 1D Straight-Leg Model for a high value of cartilage viscosity and for a low value of cartilage viscosity. We observe a great difference in the response predicted at the ankle dependent upon the knee cartilage value. However, the response at the hip is relatively unchanged. It should be noted that with more realistic parameter values the response at the hip may be affected to a greater degree. As a result, we may be able to detect changes in the knee viscosity with only a single sensor at the ankle. These results are promising and suggest that this model as good potential to be used to identify the cartilage viscosity. We therefore highly recommend further refinement and investigation of this model.

Proposed experiment

In this section, we propose an experimental procedure using the 1D Leg Model that could be applied to determine the viscosity of the cartilage in the knee. Our hypothesis is that the viscosity of the cartilage in the knee is correlated with degree of knee osteoarthritis and therefore determination of the knee viscosity, η_K, will assist in diagnosis.

In the experiment, we propose that accelerometer sensors are attached to the ankle and hip as in the gait experiments, with the sensors precisely aligned with the leg. The patient should then sit down, remove any shoes or footwear, and place their straightened leg onto a stand such that their leg is parallel with the floor. This ensures that it clear in which direction gravity is acting so that this can be easily factored out of the sensor data. The patient should aim to remain as still as possible throughout the experiment. After a few seconds after starting the recording with IMU, a known force should be applied to the bottom of the patient's foot. This could perhaps be done by attaching a ball of a chosen mass to a swing, holding it horizontally, then releasing it. At the bottom of the swing, the ball will make contact with the foot, thus exerting a force on it. It is simple to calculate this force by applying Newton's laws of motion to a swing. Both the accelerometer at the ankle and the hip will register an acceleration. Once the response has died down, the recording of the data can be stopped.

The described experiment will result in a time series for the acceleration at the ankle and the hip. We can then use the 1D Leg Model with the known force input. The 1D Leg Model will provide a prediction for the acceleration at both the ankle and hip. However, the model output will likely not match the experimental data for the chosen viscosity. By running the model with different values of η_K, that is the knee viscosity, one may find a value of η_K that leads to an accurate prediction of the experimental data. This process of choosing the 'best' η_K can be done systematically using mathematical optimization. This value of η_K is the knee viscosity that we have inferred from the data. The health of a patient can then be determined by comparing this value with the values of η_K obtained from healthy people and patients with damaged knees by this same method.

3.3.3 Two-segment leg model

In this section, we introduce the two-segment leg model. Following the approach presented in Rao (2013) we consider the leg consisting of two segments, the lower leg and the upper leg, and take into account joint-moments acting at the hip, knee, and ankle. The motivation for the two-segment leg model is to describe human gait dynamics by considering the joint-moments working together.

In the two-segment leg model we make several assumptions which are reasonable for kinetic gait modeling (see for example Ewins and Collins (2014)). Namely, we treat the lower and upper parts of the leg as two rigid bodies with a fixed length. Moreover, both segments are assumed to have point masses (the center of mass) to which the external forces (gravity) are applied. Consequently, mass moments of inertia remain constant. We consider one internal forcing in the hip given by the hip torque. The knee is modeled as a spring that joins the two segments.

The dynamics can be described as dynamics of a double pendulum during its swing phase, where the upper pendulum corresponds to the upper part of a leg and lower pendulum corresponds to the lower part of a leg.

We derive the equations for the double pendulum dynamics in terms of the angular orientations θ_1 and θ_2, as shown in the Figure 3.13, using the Lagrangian approach. From simple geometric observation we find the following relations between coordinates and angles:

$$
\begin{aligned}
x_1 &= \frac{l_1}{2}\cos\theta_1, \quad y_1 = \frac{l_1}{2}\sin\theta_1; \\
x_2 &= \frac{l_2}{2}\cos\theta_2 + 2x_1, \quad y_2 = \frac{l_2}{2}\sin\theta_2 + 2x_2; \\
x &= l_2\cos\theta_2 + 2x_1, \quad y = l_2\sin\theta_2 + 2x_2,
\end{aligned}
$$

where l_i is the length of the segment, the center of mass of the segment is at (x_i, y_i) for $i = 1, 2$, and (x, y) are coordinates of the hip.

With these relations, we can write down the Lagrangian of the system. We include rotational energy in the kinetic energy, where we denote by I_i the moment of inertia of the segment i. We also assume that the lower and upper part of the pendulum are connected by a

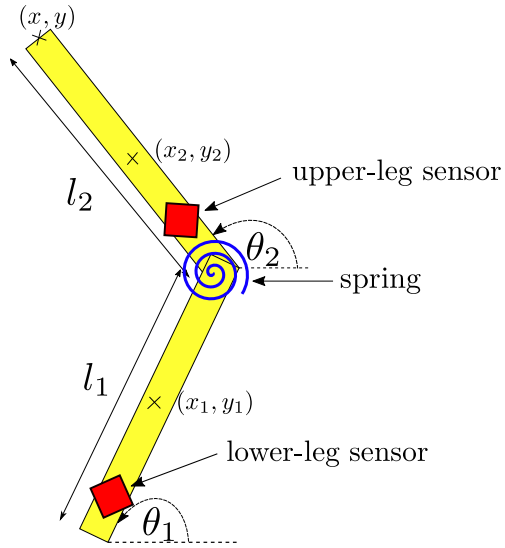

Figure 3.13: Schematic of two-segment leg model

spring with stiffness k which gives the term $\frac{1}{2}k(\theta_2-\theta_1)^2$ in the potential energy. Hence, the Lagrangian is

$$\begin{aligned}
L &= T - U \\
&= \frac{1}{2}m\left[l_1^2\dot{\theta}_1^2 + l_2^2\dot{\theta}_2^2 + 2l_1l_2\dot{\theta}_1\dot{\theta}_2\cos(\theta_1-\theta_2)\right] \\
&\quad + \frac{1}{2}m_2\left[l_1^2\dot{\theta}_1^2 + \frac{1}{4}l_2^2\dot{\theta}_2^2 + l_1l_2\dot{\theta}_1\dot{\theta}_2\cos(\theta_1-\theta_2)\right] \\
&\quad + \frac{1}{8}m_1l_1^2\dot{\theta}_1^2 + \frac{1}{2}I_1\dot{\theta}_1 + \frac{1}{2}I_2\dot{\theta}_2 \\
&\quad - mg(l_1\sin\theta_1 + l_2\sin\theta_2) - m_2g(l_1\sin\theta_1 + \frac{l_2}{2}\sin\theta_2) - m_1gl_1\sin\theta_1 \\
&\quad - \frac{1}{2}k(\theta_2-\theta_1)^2,
\end{aligned}$$

where m_i is the mass of the segment $i = 1, 2$ and m is the mass of the hip.

We assume the behaviour of the system to be non-conservative because of frictional forces acting in the knee. This leads to introducing the Rayleigh dissipation function

$$R = \frac{1}{2}c\left(\dot{\theta}_1 - \dot{\theta}_2\right)^2.$$

Another way of introducing the dissipation into the model is to assume that a damping element is attached in parallel to the spring at the knee. Hence, we refer to the constant c either as the damping or dissipation coefficient.

Now we have all the ingredients to write down the Lagrange equations of motion in the same way as it done in Rao (2013). The only one simplification we do is we assume the resting angle of the knee to be equal to π, but if one needs it is straightforward to incorporate another angle. Eventually, the Lagrange equation for the lower leg is

$$\begin{aligned}
&\ddot{\theta}_1\left[l_1^2\left(m + m_2 + \frac{m_1}{4}\right) + I_1\right] + \ddot{\theta}_2 l_2^2\cos(\theta_1-\theta_2)\left(m + \frac{m_2}{2}\right) \\
&\quad + \dot{\theta}_2^2 l_2^2\sin(\theta_1-\theta_2)\left(m + \frac{m_2}{2}\right) + gl_1\cos\theta_1\left(m + m_2 + \frac{m_1}{2}\right) \\
&\quad + k(\theta_2-\theta_1) + c\left(\dot{\theta}_2 - \dot{\theta}_1\right) = 0,
\end{aligned} \tag{3.5}$$

and for the upper leg, taking into account the hip torque T_{hip} - the only force acting on the upper-leg segment.

$$\begin{aligned}\ddot{\theta}_2 \left[l_2^2 \left(m + \frac{m_2}{4}\right) + I_2\right] + \ddot{\theta}_1 l_1^2 \cos(\theta_1 - \theta_2) \left(m + \frac{m_2}{2}\right) \\ - \dot{\theta}_1^2 l_1^2 \sin(\theta_1 - \theta_2) \left(m + \frac{m_2}{2}\right) + g l_2 \cos\theta_2 (m + m_2) \\ - k(\theta_2 - \theta_1) - c\left(\dot{\theta}_2 - \dot{\theta}_1\right) = -T_{hip}.\end{aligned} \tag{3.6}$$

As mentioned before, we use the double pendulum to describe the dynamics of a gait during the swing phase. During the stance, as described in Rao (2013), the entire leg is treated as a point mass, and the only force acting is gravity in the vertical direction. Hence, the equations of motions are:

$$\begin{aligned}\ddot{x} &= 0 \\ \ddot{y} &= -g.\end{aligned} \tag{3.7}$$

Model parameters

Two parameters of the model are related to the properties of the knee, namely, the spring stiffness k and the dissipation coefficient c. The main goal is to fit these parameters when we exploit the time-dependent angle in the ankle θ_1 as input for the model and the corresponding angle in the knee θ_2 as output. Hence, we treat variable θ_1 as given through data from the lower-leg sensor and so we do not solve the differential equation for θ_1.

Other than k and c, the model incorporates eight parameters which can be estimated individually for each person, which we describe in the table below. As a simplification, the hip torque is considered to be a constant in this model.

Numerical method

We investigate a numerical method that estimates parameters of a knee based on given time series of ankle and knee angular orientations. The equations for the two-segment leg model are derived in terms of these orientations (θ_1 and θ_2) as variables. Now we aim to infer the parameters for which the model produces desired knee angular orientation

θ_2 (output) for given ankle angular orientation θ_1 (input). Therefore, for known angles θ_1, we numerically solve second-order equation (3.6) for θ_2. In order to do so, we first transform this second-order ODE into a system of two first-order ODEs and then use MATLAB solver ODE45 to solve the resulting system. For initial conditions $\theta_2(0)$ and $\theta_2'(0)$ we have used the data from the knee sensor. We note that, in order to simplify the numerical analysis, the stance phase of the gait is neglected, so we did not take equations in (3.7) into account.

Numerical experiment

The data that we need for the numerical experiment is time series of the angular orientations of the ankle and the knee. In the previous experiments (Section 3.4) the sensors were placed on the ankles and the lower back, which does not provide the necessary data for the knee. Thus, we performed our experiments where we used one more sensor attached just above the knee (Section 3.4.1). To extract the required angular orientations one has to map the data to the global coordinate system as it is described in Section 3.2.2.

To perform a simple numerical experiment we consider the angular velocities around the z-axis in the data from gyroscope in IMU. We used the data from our walking experiments (Section 3.4.1). Figure 3.14 shows the angles obtained by discrete-time integration of the angular velocities (left) and the periodogram for the series of angles (right). Figure 3.14 gives us two useful insights. Firstly, we notice a drift downwards which is a known problem with the gyroscope measurements. Our second observation is that the data has a simple periodic pattern and shows much less noise than the accelerometer data. In the periodogram we see two main frequencies for the ankle (≈ 0.7 Hz and ≈ 1.6 Hz) and one main frequency for the knee (≈ 0.7 Hz). Low frequencies (< 0.5 Hz) are related to the drift and should be filtered out.

Meaning of the parameters

By fitting the parameters k and c to fit the numerical solution, we noticed that the damping coefficient c determines the global dynamics

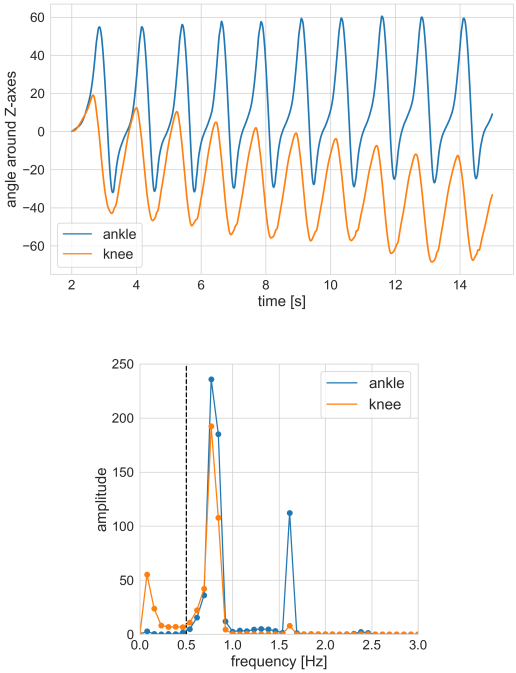

Figure 3.14: Time series for angular orientations around the z-axis of the ankle and knee and corresponding periodogram.

of the model. For example, as seen in the Figure **??** on the left, if the parameter c is small enough, the qualitative behaviour of the model fits to the data. However, if the parameter c is greater than some critical value, than the amplitude of the model's solution is increasing.

Proposed experiment

We propose an experiment in which the patient walks for ten metres with accelerometers attached to each ankle and just above a knee. Then, a similar data analysis, as described in the subsections before,

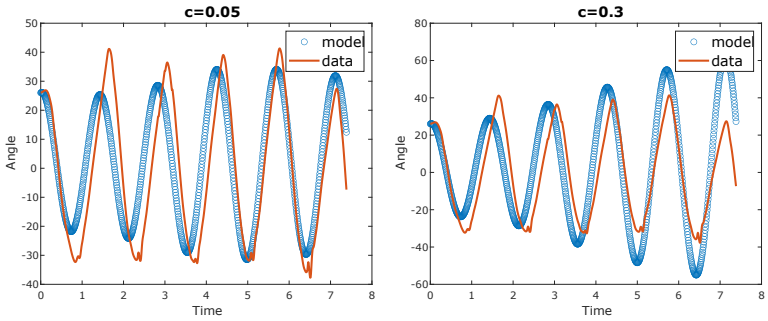

Figure 3.15: Fitting the data for θ_2 from the sensor attached on Rico's knee to the numerical solution

should be performed in order to fit the parameters k and c. One can find the parameters k and c by running the simulation with various choices of parameters until the difference between the numerical solution and the data is small enough. However, a better approach would be to use optimization algorithms to find the optimal values of the parameters which would fit best into the data. It would be interesting to compare the values of these parameters for healthy patients and for the patients suffering from knee osteoarthritis.

3.4 Experiments

Gerbrands kindly offered us to use his sensors. This enabled us to perform several experiments and analyse our own data. Firstly, we let different people walk with sensors on the ankle, just above the knee, and on the lower back. Secondly, since the human body is complex we attempted to do a more controlled experiment by using wood and foam.

3.4.1 Walking experiments

We let two different people walk over a distance of approximately ten meters. The IMU sensors were attached with tape to the ankle, just

above the knee and to lower back. We let people walk on bare feet such that we have no noise in the data caused by the type of footwear. Figure 3.16 shows pictures of the positions of the sensors and one person walking.

Figure 3.16: On the left we show a picture of Mara Smeele walking. The position of the sensors on the ankle and just above the knee is visible. The picture on the right shows the position of the sensor on the lower back.

In order to obtain a better feeling of the effects on the data of different people walking differently, we repeated on a small scale the

experiment that Gerbrands does in his lab. We attached sensors to the ankle and the hip of two different people walking and compared the results. Figure 3.17 shows the acceleration over time measured by the IMU sensors for two different people walking. The blue line is the acceleration along the longitudinal axis, which is the axis aligned with the leg, and the orange line is the acceleration in the transverse direction. Figure 3.2 in the introduction shows the direction of the axes. In Figure 3.17 the upper graphs are of the first person walking and the lower graphs of the second person walking. The graphs on the left are data from the sensors on the ankle and the graphs on the right are data from the sensors on the lower back. Both persons show a regular walking pattern, but the patterns differ a lot. When we compare the data we see that the acceleration of the first person is much bigger than the acceleration of the second person. From this data we can see that different people walk very differently. This observation from our small sample implies that it might be very hard to draw any conclusions on the state of the cartilage from the data of the sensors on the ankle and the lower back.

In the introduction we explained that Gerbrands did not put any sensors just above the knee because of the possible influence of the soft tissue. However, for the two-segment leg model we needed data about the angular orientation of the knee. Therefore, we decided to do experiments with sensors just above the knee. Fortunately, there was not too much noise from the soft tissue and we use this in Section 3.3.3 which gives some interesting results.

3.4.2 Wood and foam

One of the questions posed by Gerbrands was whether material properties of the cartilage in the knee can be inferred from IMU sensor data. Although this is a question about the knee, it is confounded by other issues:

- The human body is a large and complicated object, with many parts of different physical properties, and therefore any signal from the cartilage is perturbed by signals from the rest of the body;

- The human gait is in itself a complicated movement, with many joints and muscles working together.

In an attempt to separate the issues, we therefore posed the question whether material properties of cartilage can be inferred from sensor data in a 'perfect' situation without these confounding factors.

Setup. To assess this we performed experiments on a model system consisting of wooden rods connected by a foam damper. The rods were laid on a table in contact with each other, with some foam squeezed between the two. One rod was held down by hand and struck by a hammer. After the impact, the first rod quickly moved a short distance ($\approx 1\,\mathrm{cm}$) while being held down by hand, while the second rod was free to slide over the table. Figures 3.18 and 3.19 show the setup.

We performed a number of different experiments, but here we only report on two: one experiment with a thick padding of foam between the two rods, and one without any foam; in this latter experiment the two rods touched wood-on-wood. Figure 3.20 shows a number of measurements.

Observations. The blue lines show the acceleration of the first rod—the rod that is struck by the hammer. All graphs show a remarkable *negative* acceleration peak (i.e., a deceleration peak) in the first rod, but practically no *positive* acceleration in the first rod. Since this negative acceleration has to have been preceded by positive acceleration, we interpret this as indicating that the positive acceleration in the first rod as result of the hammer strike happens in such a short time that the IMU is unable to capture it.

In the top two graphs, with foam padding, the deceleration peak in the first rod is matched by an acceleration peak in the second rod. We interpret this as an indication that the padding acts as a soft spring, leading to a relatively slow increase and then decrease in force between the two rods as the foam first compresses and then decompresses. By Newton's third law this leads to two equal and opposite peaks in the diagram.

On the other hand, without foam, the acceleration peak of the second rod also is hardly visible; we interpret this as an indication that the wood–on–wood contact causes very rapid acceleration in both rods, and therefore both acceleration peaks are too rapid for the IMU.

In all graphs, after the initial peaks a weak deceleration is visible in the second rod; this deceleration remains approximately constant over a period of roughly half a second (this period is indicated in the top-left graph, but the same period is visible in the three other graphs as well). We interpret this constant-level deceleration as an instance of Coulomb friction: the force remains constant while there is motion, and abruptly drops to zero upon stand-still.

Conclusions from these experiments. Based on the observations and interpretations above, we draw the following conclusions.

1. Holding down the first rod served the purpose of preventing the rods from flying around, but it interferes with the dynamics; in a new experiment we should avoid this.

2. The question whether we can infer the properties of the padding from IMU measurements remains open. It is true that the top and bottom rows in Figure 3.20 are significantly different; but for a large part this is due to the applied acceleration being too fast for the IMU to measure.

If these experiments were to be done again (and better), then we would advise to set them up as follows:

1. The aim of the experiment would remain the same: determine whether these specific sensors are capable of characterizing the material properties of the 'cartilage' in the 'knee', in what is otherwise the best possible setup.

2. One could take two pieces of wood or other material to match the mass of the thigh bone and the shin bone; the elastic properties do not seem to matter much, as long as the material is sufficiently stiff (see the discussion above). The IMU sensors would be rigidly fixed to the 'bones'.

3. The cartilage would again be modelled by different types and thicknesses of foam; the challenge would be to recover the properties of the foam from the IMU measurements.

4. The impact should be repeatable; if a specialized device is not available, then for instance a weight hitting the wood by falling would probably suffice.

5. The impact needs to be carefully chosen: it has to be short in order to resemble an instantaneous impact for the foam, but slow enough for the IMU sensors to be able to capture it through the movement of the wood. In fact, satisfying these competing requirements may be the main challenge. In order to vary the speed of impact the wood can be padded, at the impacted end, by different amounts of padding.

3.5 Conclusion and recommendations

In our study, we took several approaches: we analysed the provided data, we performed our own experiments, studied literature and we formulated two models. Here, we provide a summary of our recommendations.

First, some observations from the data and our analysis of that. In the data analysis that was performed by Gerbrands, only the acceleration data was used while the IMU also contains a gyroscope that generates rotational velocity data. Moreover, the data that is measured is in the frame of reference of the leg: the orientations of the sensors are chosen such that these measure the longitudinal and transversal components of acceleration as shown in Figure 3.2. It turns out this is not a convenient frame to work in since it changes when people walk. Finally, we observed that the data was provided to us in 148 Hz while the IMUs can generate data of 470 Hz. This leads to the following recommendations:

1. Use data of the full 470 Hz of the IMU sensors can generate.

2. Transform the data to a global coordinate system.

3. Combine the acceleration data with the gyroscope data, this will result in less noise.

In the frequency domain analysis in Section 3.2.3 we suggest to use the coherence for examining the relation between the signals from the ankle and the lower back. However, we did not have enough data to work with, hence, we recommend

4. Apply coherence analysis to large amount of measurements from people with healthy and damaged cartilage.

In the study of the vibration plate in Section 3.2.4 we found that the natural frequency of the body is around 7 Hz however this is also used as the frequency of the vibration plate. This will lead to resonance and therefore we recommend

5. In case you want to use the vibration plate set the plate to frequencies higher than 7 Hz.

Then, in Section 3.3, we formulate two models and we think it would be worthwhile to study these models in more detail. In Section 3.3.2 and we formulated a model for a straight leg and in Section 3.3.3 a model for a leg in motion (gait) including the bending of the knee. In both cases we formulated specific experiments that can be done and from these the condition of the knee can be inferred. So we recommend to

6. Analyse the models in Sections 3.3.2 and 3.3.3 in more detail.

7. Perform the experiments formulated in Section 3.3.2 and Section 3.3.3, this will lead to conclusions about the condition of the knee cartilage.

This gives a first answer to Question 2 posed in Section 3.1.3.

Then, in Section 3.4 we performed our own experiments where in Section 3.4.2 we used wood and foam instead of people. From that we conclude

8. In case you want to do experiments with simple materials with known properties such as wood and foam, we give a whole list of recommendations for that at the end of Section 3.4.2.

Finally, we think that the question posed was very interesting and it would be worthwhile to continue the collaboration.

References

Amirkulova, F. A. (2011). "Dispersion relations for elastic waves in plates and rods". PhD thesis. Rutgers University-Graduate School-New Brunswick.

Aygün, H. et al. (2015). "Sound Propagation through bone tissue". In: *Proceedings of the Institute of Acoustics* 37.2, pp. 234–238.

Baaijens, F. P. T. (1994). *Applied Computational Mechanics 1*. Eindhoven, The Netherlands: Eindhoven University of Technology.

Bendat, J. S. and A. G. Piersol (2011). *Random Data: Analysis and Measurement Procedures*. John Wiley and Sons.

Bruin, E. D. de et al. (2005). "A validity study of phase velocity measurements in spinal cord injury." In: *Journal of Rehabilitation Research & Development* 42.1.

Conrad, B. P. (2001). "The effects of glucosamine and chondroitin on the viscosity of synovial fluid in patients with osteoarthritis". PhD thesis. University of Florida.

Ewins, D. and T. Collins (2014). "Clinical Gait Analysis". In: *Clinical Engineering*. Elsevier, pp. 389–406.

Fulcher, G. R., D. W. L. Hukins, and D. E. T. Shepherd (2009). "Viscoelastic properties of bovine articular cartilage attached to subchondral bone at high frequencies". In: *BMC musculoskeletal disorders* 10.1, p. 61.

Ghosh, M. et al. (2017). "Modeling and analysis of elastic fields in tibia and fibula". In: *AIP Conference Proceedings*. Vol. 1919. AIP Publishing LLC, p. 020016.

Girrbach, R. T. et al. (2001). "Flexural Wave Propagation Velocity and Bone Mineral Density in Females With and Without Tibial Bone Stress Injuries". In: *Journal of Orthopaedic & Sports Physical Therapy* 31.2. PMID: 11232740, pp. 54–69. DOI: 10.2519/jospt.2001.31.2.54. eprint: https://doi.org/10.2519/jospt.2001.31.2.54. URL: https://doi.org/10.2519/jospt.2001.31.2.54.

Harazin, B. and J. Grzesik (1998). "The Transmission of Vertical Whole-Body Vibration To The Body Segments of Standing Subjects". In: *Journal of Sound and Vibration* 215.4, pp. 775–787. DOI: https://doi.org/10.1006/jsvi.1998.1675.

Henriksen, M. et al. (2008). "Influence of pain and gender on impact loading during walking: a randomised trial". In: *Clinical Biomechanics* 23.2, pp. 221–230.

Hörchens, L. (2010). "Imaging of material inhomogeneities with flexural waves". PhD thesis. Delft, The Netherlands: Delft University of Technology.

It'is (2010 (accessed June 2, 2020)). *Density*. URL: https://itis.swiss/virtual-population/tissue-properties/database/density/.

John, J. G. S. and R. Cameron (1999). *Roderick M. Grant Physics of the Body*.

Kok, M., J. D. Hol, and T. B. Schön (2018). "Using inertial sensors for position and orientation estimation". In: *Foundations and Trends in Signal Processing* 11.1–2, pp. 1–153. DOI: 10.1561/2000000094.

Konow, N. and T. J. Roberts (2015). "The series elastic shock absorber: tendon elasticity modulates energy dissipation by muscle during burst deceleration". In: *Proceedings of the Royal Society B: Biological Sciences* 282.1804, p. 20142800.

Madgwick, S. O. H., A. J. L. Harrison, and R. Vaidyanathan (2011). "Estimation of IMU and MARG orientation using a gradient descent algorithm". In: *2011 IEEE International Conference on Rehabilitation Robotics*, pp. 1–7.

Meyler, Z. (2018). *Knee Anatomy*. https://www.arthritis-health.com/types/joint-anatomy/knee-anatomy.

Rao, N. V. (2013). "Analysis of an actuated two segment leg model of locomotion". MA thesis. Purdue University.

Rho, J. Y., R. B. Ashman, and C. H. Turner (1993). "Youngs modulus of trabecular and cortical bone material: Ultrasonic and microtensile measurements". In: *Journal of Biomechanics* 26.2, pp. 111–119. DOI: 10.1016/0021-9290(93)90042-d.

Roetenberg, D. et al. (2005). "Compensation of magnetic disturbances improves inertial and magnetic sensing of human body segment orientation". In: *IEEE Transactions on Neural Systems and Rehabilitation Engineering* 13.3, pp. 395–405. DOI: 10.1109/TNSRE.2005.847353.

Setton, L. A., D. M. Elliott, and V. C. Mow (1999). "Altered mechanics of cartilage with osteoarthritis: human osteoarthritis and an experi-

mental model of joint degeneration". In: *Osteoarthritis and cartilage* 7.1, pp. 2–14.

Valenti, R. G., I. Dryanovski, and J. Xiao (2015). "Keeping a good attitude: a quaternion-based orientation filter for IMUs and MARGs". In: *Sensors* 15, pp. 19302–19330. DOI: 10.3390/s150819302.

Van Buskirk, W. C., S. C. Cowin, and R. N. Ward (1981). "Ultrasonic measurement of orthotropic elastic constants of bovine femoral bone". In: *Journal of Biomedical Engineering* 103.2, pp. 67–72.

Vogl, F. et al. (2016). "Reliability of Phase Velocity Measurements of Flexural Acoustic Waves in the Human Tibia In-Vivo". In: *PloS one* 11.3.

Welch, P. D. (1967). "The use of Fast Fourier Transform for the estimation of power spectra: a method based on time averaging over short, modified periodograms". In: *IEEE Transactions on Audio and Electroacoustics* AU-15.2, pp. 70–73.

Wong, B. L. et al. (2008). "Biomechanics of cartilage articulation: effects of lubrication and degeneration on shear deformation". In: *Arthritis & Rheumatism: Official Journal of the American College of Rheumatology* 58.7, pp. 2065–2074.

3.A Numerical method for 1D straight-leg model

To provide a numerical solution of the 1D straight-leg model (Section 3.3.2), we use the method of lines. We first discretize the spatial dimension using the finite-element method as described in Baaijens (1994). We then convert the resulting system of second-order time-dependent ordinary differential equations (ODEs) into a system of first-order ODEs and use MATLAB's inbuilt ODE solver: ODE45. The

system of linear equations is given by:

$$\underbrace{\int_0^L \mathbf{\Phi}_x A(x) E(x) \mathbf{\Phi}_x^T dx}_{K} \mathbf{U} + \underbrace{\int_0^L \mathbf{\Phi}_x A(x) \eta(x) \mathbf{\Phi}_x^T dx}_{B} \dot{\mathbf{U}} +$$

$$\underbrace{\int_0^L \mathbf{\Phi}(x) \rho(x) A(x) \mathbf{\Phi}(x)^T dx}_{M} \ddot{\mathbf{U}} = \underbrace{\int_0^L \mathbf{\Phi}(x) f(x,t) dx}_{\mathbf{F}(t)}$$

$$K\mathbf{U} + B\dot{\mathbf{U}} + M\ddot{\mathbf{U}} = \mathbf{F}(t) \tag{3.8}$$

where L is the total length of the one-dimensional domain, $\mathbf{\Phi}(x)$ is a column containing n shape functions $\phi_i(x)$, $\mathbf{\Phi}_x$ is the column of derivatives of the shape functions with respect to the axial coordinate x, $\mathbf{U}$ is the column containing the nodal displacements, $\dot{\mathbf{U}}$ is a column containing the nodal velocities and $\ddot{\mathbf{U}}$ is a column containing the nodal accelerations. $F(x,t)$ is the applied force per unit length, and when assembled to vector $\mathbf{F}(t)$, nodal forces can be set to the corresponding entries. K, M and $\mathbf{F}$ will be assembled from their element matrices, $K = \mathop{\mathrm{A}}_{e=1}^{n_{\mathrm{el}}} K^e, M = \mathop{\mathrm{A}}_{e=1}^{n_{\mathrm{el}}} M^e$ and $\mathbf{F} = \mathop{\mathrm{A}}_{e=1}^{n_{\mathrm{el}}} \mathbf{F}^e$.
Finally the system of equations can be phrased as an initial value problem.

$$\ddot{\mathbf{U}} \quad = \quad M^{-1}(\mathbf{F} - K\mathbf{U} - B\dot{\mathbf{U}}) \tag{3.9}$$

from which the nodal displacement column $\mathbf{U}$ can be obtained. After solving $\mathbf{U}(x)$ the element stresses can be obtained from equation (3.3b).

Parameter	Units	Description	Value
L_{LL}	m	Length of bone in lower leg	0.5
L_K	m	Length of cartilage in knee	6×10^{-3}
L_{UL}	m	Length of bone in upper leg	0.5
L_{UB}	m	Length of upper body	0.5
ρ_{LL}	$\mathrm{kg\,m^{-3}}$	Density of bone in lower leg	1900
ρ_K	$\mathrm{kg\,m^{-3}}$	Density of cartilage in knee	1000
ρ_{UL}	$\mathrm{kg\,m^{-3}}$	Density of bone in upper leg	1900
ρ_{UB}	$\mathrm{kg\,m^{-3}}$	Average upper body density	1900
A_{LL}	$\mathrm{m^2}$	Cross-sectional area of bone in lower leg	0.027
A_K	$\mathrm{m^2}$	Cross-sectional area of cartilage in knee	0.019
A_{UL}	$\mathrm{m^2}$	Cross-sectional area of bone in upper leg	0.027
A_{UB}	$\mathrm{m^2}$	Average cross-sectional area of conducting material in upper body	0.027
E_{LL}	$\mathrm{kg\,m^{-1}\,s^{-2}}$	Young's Modulus of bone in lower leg	17×10^9
E_K	$\mathrm{kg\,m^{-1}\,s^{-2}}$	Young's Modulus of cartilage in knee	12×10^6
E_{UL}	$\mathrm{kg\,m^{-1}\,s^{-2}}$	Young's Modulus of bone in upper leg	17×10^9
E_{UB}	$\mathrm{kg\,m^{-1}\,s^{-2}}$	Average Young's Modulus of conducting materials in upper body	17×10^9
η_{LL}	$\mathrm{kg\,m^{-1}\,s^{-1}}$	Viscosity of bone in lower leg	2×10^9
η_K	$\mathrm{kg\,m^{-1}\,s^{-1}}$	Viscosity of cartilage in knee	10^2
η_{UL}	$\mathrm{kg\,m^{-1}\,s^{-1}}$	Viscosity of bone in upper leg	2×10^9
η_{UB}	$\mathrm{kg\,m^{-1}\,s^{-1}}$	Averaged viscosity conducting materials in upper body	2×10^9

Table 3.1: Estimated parameter values for the 1D Leg Model.

Parameter	Units	Desciption	Proposed value
l_1	m	Length of lower-leg segment	1
l_2	m	Length of upper-leg segment	1
m_1	kg	mass of lower-leg segment	1
m_2	kg	mass of upper-leg segment	1
I_1	kgm^2	intertia of lower-leg segment	0.5
I_2	kgm^2	intertia of upper-leg segment	0.5
k	$\mathrm{kgm}^2\mathrm{s}^{-2}$	spring coefficient	12.7
c	$\mathrm{kgm}^2\mathrm{s}^{-1}$	damping coefficient	0.05
θ_{ref}	rad	resting angle	$2/3\,\pi$
T_{hip}	$\mathrm{m}^2\mathrm{kgs}^{-2}$	hip torque	0.7

Table 3.2: Parameters in the two-segment leg model

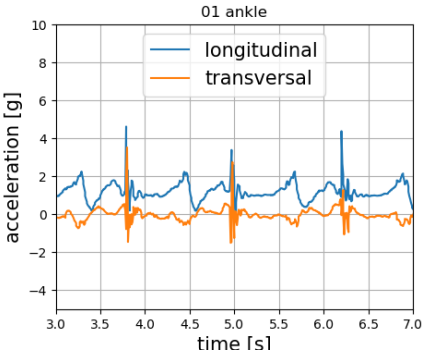
01 ankle
longitudinal
transversal
acceleration [g]
time [s]

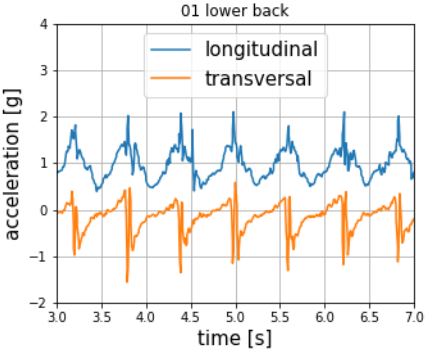
01 lower back
longitudinal
transversal
acceleration [g]
time [s]

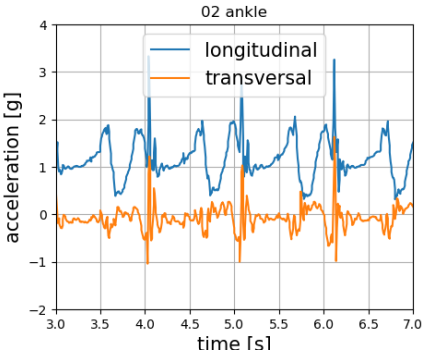
02 ankle
longitudinal
transversal
acceleration [g]
time [s]

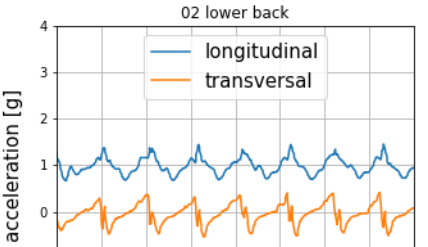
02 lower back
longitudinal
transversal
acceleration [g]

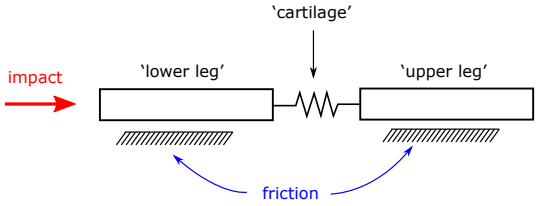

Figure 3.18: Schematic setup of the wood–and–foam experiment.

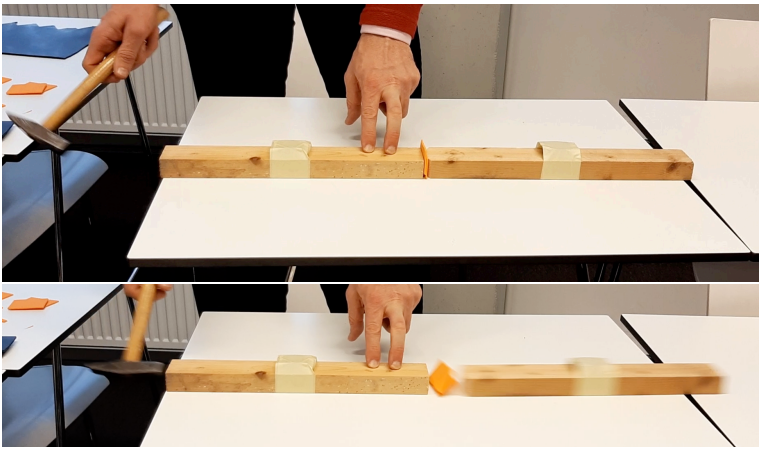

Figure 3.19: A single experiment, before and after the impact.

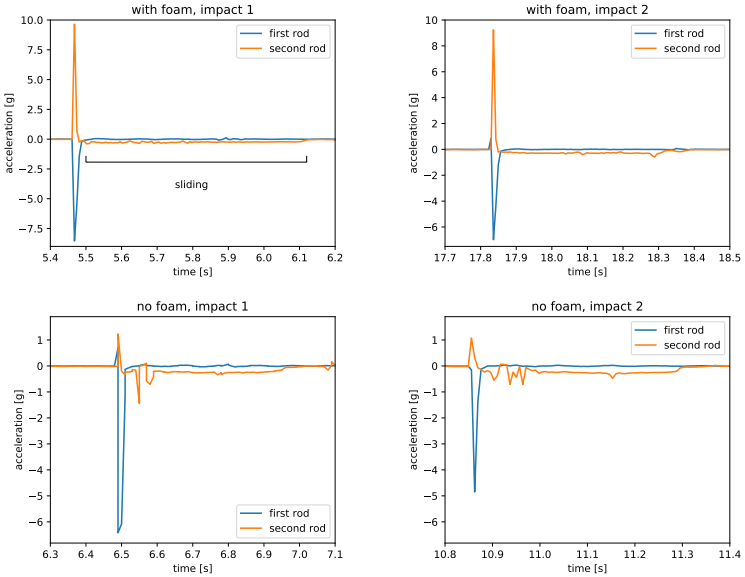

Figure 3.20: Two sets of experiments. Top row: wood-on-wood; bottom row: foam padding.